Vesicular release of neurotransmitters: Converting amperometric measurements into size, dynamics and energetics of initial fusion pores

Article *in* Faraday Discussions · November 2013

DOI: 10.1039/C3FD00028A · Source: PubMed

5 authors, including:

Frédéric Lemaître
Ecole Normale Supérieure de Paris
62 PUBLICATIONS **1,085** CITATIONS

SEE PROFILE

Irina Svir
Ecole Normale Supérieure de Paris
94 PUBLICATIONS **1,119** CITATIONS

SEE PROFILE

Faraday Discussions

RSC Publishing

Cite this: *Faraday Discuss.*, 2013, **164**, 33

PAPER

View Article Online
View Journal | View Issue

Vesicular release of neurotransmitters: converting amperometric measurements into size, dynamics and energetics of initial fusion pores†

Alexander Oleinick, Frédéric Lemaître, Manon Guille Collignon, Irina Svir and Christian Amatore*

Received 4th March 2013, Accepted 15th March 2013
DOI: 10.1039/c3fd00028a

Amperometric currents displaying a pre-spike feature (PSF) may be treated so as to lead to precise information about initial fusion pores, *viz.*, about the crucial event initiating neurotransmitter vesicular release in neurons and medullary glands. However, amperometric data alone are not self-sufficient, so their full exploitation requires external calibration to solve the inverse problem. For this purpose we resorted to patch-clamp measurements published in the literature on chromaffin cells. Reported pore radii were thus used to evaluate the diffusion rate of neurotransmitter cations in the partially altered matrix located near the fusion pore entrance. This allowed an independent determination of each initial fusion pore radius giving rise to a single PSF event. The statistical distribution of the radii thus obtained provided for the first time an experimental access to the potential energy well governing the thermodynamics of such systems. The shape of the corresponding potential energy well strongly suggested that, after their creation, initial fusion pores are essentially controlled by the usual physicochemical laws describing pores formed in bilayer lipidic biological membranes, *i.e.*, they have an essentially lipidic nature.

Introduction

In exocytotic cells neurotransmitters are transported inside vesicles, in which they are densely packed.[1] Whenever release into the extracellular environment is needed, the gated-entrance of calcium ions into the cytoplasm initiates a process stimulating primed vesicles to fuse with the cytoplasmic cell membrane. This fusion begins through the opening of a nanometric liquid channel connecting the vesicle with the extracellular space so that neurotransmitters may be released towards a target cell (synaptic cells: neurons and nerve terminals) or into

Ecole Normale Supérieure, Département de Chimie, UMR ENS-CNRS-UPMC 8640 "PASTEUR", 24 rue Lhomond, 75005 Paris, France. E-mail: christian.amatore@ens.fr; Tel: +33-(0)1-4432-3388

† Dedicated to the late Professor Louis Nadjo, a lamented friend and colleague but most of all Christian Amatore's first tutor in experimental electrochemistry.

circulating fluids (gland cells).[1] It is commonly agreed that, irrespective of the cell nature (synaptic or medullar gland cell), this central process occurs through several distinct steps initiated by the flow of calcium ions into the cell cytoplasm. Calcium ion entry promotes the assembly of specific proteins (SNAREs) anchored in the cell and vesicle membranes. Progressive tightening of the SNAREs complexes forces the vesicle to enter in close contact with the cell membrane (the "docking" stage, Fig. 1). After docking, a narrow pore of nanometric dimensions, named the initial fusion pore, spontaneously forms across the two membranes so that the vesicle content may diffuse into the synaptic cleft (synaptic cells) or into the circulating fluids (gland cells).

Unless the initial fusion pore closes after some duration (as is believed to occur in neurons, or has been observed during "kiss and run" events for gland cells)[3] it eventually suddenly quickly enlarges through a rapid flow of the vesicle bilayer membrane into that of the cell.[4a] This process, named "full fusion", is completed within a few milliseconds and unmasks a larger fraction of the vesicle matrix surface, thus allowing a massive release compared to the extremely limited one which may occur through the small initial fusion pore (Fig. 1).

Since its first characterization by patch-clamp techniques,[5,6] the initial fusion pore has stimulated numerous studies, echoing its crucial importance in initiating the whole process as well as crucial fundamental demands concerning its size, nature and energetics. It now seems clear that its initial formation requires the essential involvement of proteins such as SNAREs and calcium ions, which permit the two membranes to overcome their repulsion and come into sufficiently close contact to initiate a local merging.[7,8] Many experiments support this view, and in particular, the exocytotic frequency is drastically decreased when SNAREs are disabled, *e.g.*, after botulic treatment.[9,10] However, it seems that other local cellular sub-structures (*e.g.*, the surface cytoskeleton,[11] molecular motors, *etc.*) may also be involved during this phase, since exocytotic events appear to occur only at a few precisely localized spots on the cell membranes.[4b,12] Therefore there is no doubt that the initial pore formation involves a series of organized bio-structures on

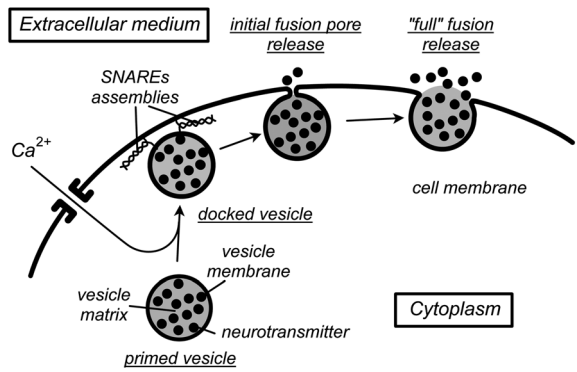

Fig. 1 Schematic representation of the main sequential stages of a vesicular exocytosis event. Neurotransmitter molecules are represented by filled circles initially contained inside the fusing vesicle. Note that, for the sake of simplicity, possible SNAREs assemblies existing in the fusion stages after creation of the initial fusion pore are not shown since this is still a matter of debate; similarly, only a toroid topology is shown for the "full" fusion stage but the vesicle opening may be connected to that in the cell membrane through a lipidic tube (see Fig. 6 in the Appendix).[2]

which specific bio-machineries operate. Nevertheless, there is still no agreement about the very nature of the initial fusion pore after it has been created: does it involve purely lipidic components? proteic ones? any combination thereof? In other words, does it obey purely physicochemical laws or remain controlled biologically, at least in part?[13,14]

The present work aims to introduce a new approach for experimental characterization of the initial fusion pore dimensions and providing statistical elements about its energy since such data are critical for assessing its very nature. To the best of our knowledge, most of the quantitative experimental information about the initial biological fusion pores is topological and stems from two main sources: patch-clamp experiments (topological information reconstructed from dynamic events);[5–7,15–17] or high-power electron microscopy of prepared cell slices (direct topological observation from events "frozen" at different completion stages during the preparation).[18] Both techniques concur to establish that initial fusion pore radii are around 1.2 nm.

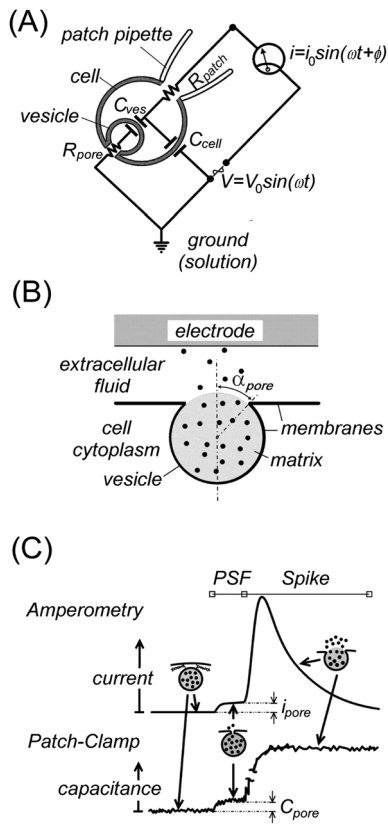

Fig. 2 Schematic principles of patch-clamp (A) and amperometry (B) and comparison of their respective measurements of a vesicular exocytotic event (C). (A) shows a "whole cell" patch-clamp configuration but several other configurations may be used.[5–7] (B) indicates the geometry of amperometric measurements in the "artificial synapse" configuration[19] and defines the opening angle, α_{pore}, characterizing the size of the pore at any fusion stage (this is shown for a toroid connection; see Fig. 6 in the Appendix for a tubular one[2]). In (C) the subscript "pore" stands for "initial fusion pore".

Patch-clamp measurements rely on dynamic measurement of impedance changes induced locally in the cell membrane by pore opening. These data are extracted in terms of their capacitive and resistive components, recorded as functions of time at an adequate frequency, on the basis of models initially developed by E. Neher *et al.* for the investigation of ion channels (see Fig. 2A).[15–17] Briefly, the vesicle and its opening fusion pore are represented by an equivalent electrical RC circuit in which the resistive component changes are mainly those of the liquid tube present in the pore and in the vesicle, while the capacitive ones mostly reflect the excess of surface area provoked by the pore opening, *viz.*, is related to the pore radius (Fig. 2A).[20] These are converted into topological information through independent calibration.[21] Based on such investigations it is now widely accepted that fusion pores suddenly open (*i.e.*, at submillisecond durations from the closed stage to complete opening).[22] Note that the experimental range of observed pore diameters (*viz.*, 2.4 ± 0.7 nm; 68% confidence)[22] is much wider than the accuracy of patch-clamp measurements. Such a dispersion of measured values then suggests that the initial fusion pores display a rather wide intrinsic distribution of sizes, a fact that strongly mitigates against a purely proteic nature.

Initial fusion pores are also observable by amperometry, *viz.*, through monitoring electrochemically the fluxes of released neurotransmitters through their rapid quantitative collection by their Faradaic oxidation at a carbon fiber ultramicroelectrode surface positioned at *ca.* 100 nm from the cell membrane so as to create an "artificial synapse" (Fig. 2B).[19] The full fusion release stage (see Fig. 1) is featured by an intense amperometric spike whose rising section characterizes mostly the exponential pore enlargement rate while its smoother descending branch represents mainly the progressive diffusional release of molecules from inside the vesicle (Fig. 2C).[23–25] More precisely, the exponential time decay of the amperometric current during this latest phase establishes that the pore radius has already completed its rapid growth phase and reached a constant value.[26,27] About 30% of such spikes are preceded by comparatively small specific current features (termed a "foot" or "pre-spike-feature", PSF) whose diffusional characteristics point to the fact that they represent diffusion of neurotransmitters through the nanometric initial fusion pore.[28–30] Diffusion laws are well established,[31] so one may think that PSF currents could be precisely deconvoluted from amperometric data so as to provide a fine description of the initial fusion pore topology.[32] Should it be feasible, amperometry could become a method of choice for the statistical investigation of initial fusion pore dimensions, since a single amperometric trace monitored from a single stimulated cell already offers several hundred PSF events with different characteristics (*i.e.*, different durations, plateau intensities and shapes).

To develop such an amperometric approach one may rely on our previous theory of diffusion from spherical bodies impermeable to diffusing molecules over a fraction of their surface.[27] Yet, this would suppose knowing *a priori* either the rate of diffusion across the inside of the vesicle, $\kappa = D_{ves}/R_{ves}^2$ (where D_{ves} is the diffusion coefficient inside the vesicle and R_{ves} the radius of the vesicle), or the maximum cone angle α_{open}^{max} (see Fig. 2B) limiting the diffusion-permeable surface area when the fusion is complete, or the concentration of neurotransmitter, C_{ves}^{rel}, contained initially inside the vesicle and effectively released at the end of the process.[27] However, if the quantitative and kinetic information contained in the amperometric spike provides a useful relationship between these key parameters (*e.g.*, see below eqn (1)),[27b] it cannot give access to any one of these three crucial values without blunt

assumptions based on mean values.[23,24,33] Nevertheless, the large variability of vesicular events (see below) and present doubts about the completeness of full fusion[23,24] (*i.e.*, does α_{open}^{max} really approach 180°?) preclude using mean values for the treatment of any particular event (note that hereafter, and in all Figures, angle values are always reported in degrees unless specified otherwise so that, when necessary, their conversion into radians requires a re-scaling by the factor $\pi/180$).

Hence, solving the inverse problem at hand requires an independent entry. We wish to show hereafter that comparing patch-clamp and PSF amperometric data provides such an external entry. This permits a quantitative access to the diffusion rate κ and therefore allows the extraction of topological information from individual PSF currents. Note that such a strategy does not differ conceptually and practically from that used in extracting pore dimensions from impedance measurements. Indeed, this also requires external input, *viz.*, independent calibrations of differential capacitances and resistivities.[21]

The following analysis is developed in the context of dense core vesicles, such as those of chromaffin cells which are investigated amperometrically here, but it may be readily adapted to other situations provided that precise patch-clamp and amperometric data are available.

Results and discussion

Position of the problem

It is clear that α_{open}^{max} cannot be known *ex nihilo* from a current trace unless it is hypothesized that full fusion is total, *viz.*, that $\alpha_{pore}^{max} = 180°$, as some of us have done previously[23,24] following prevailing views about full fusion at the time when these former works were performed.[4a] However, this is now an increasingly questioned issue.[13,14,34]

Alternatively, one could think of deriving C_{ves}^{rel} through the amperometric charge Q determined during a whole release event since $C_{ves}^{rel} = Q/[2F(4\pi R_{ves}^3/3)]$, (where F is the Faraday constant, *i.e.*, 96,485 C mol^{-1}, and the factor 2 stems from the fact that oxidation of adrenaline cation involves a two-electron process[35]). However, application of this procedure would require that the vesicle radius, R_{ves}, is known with adequate precision for the vesicle undergoing the precise event under investigation. R_{ves} could be formally obtained from coupled experiments involving simultaneous TIRFM and amperometry measurements.[36] However, at their present stage, the maximum resolution of such experiments is not yet sufficient for the precision required here. Since R_{ves} exhibits a rather large distribution,[36] this prompted us to rely on external access to κ through calibrating PSF current extraction based on published patch-clamp data on the initial fusion pore radius value (1.2 nm).[22]

Extraction of diffusional rate by comparing PSF and published patch-clamp data

In the following we consider a statistically representative series of 80 amperometric events displaying distinct pre-spike features with different shapes and current intensities covering the whole spectrum of experimental variability observed for these events. These were first analyzed as described below to extract in each case the value of the diffusion rate $\kappa = D_{ves}/R_{ves}^2$, so that the amperometric PSF current intensity agreed with the accepted mean initial fusion pore radius value.

For this purpose the theoretical approach developed previously by some of us[27] was specifically adapted to small opening angles. The whole treatment was performed in terms of angles rather than dimensions since this allowed us to by-pass the unknown value of the radius, R_{ves}, of the particular vesicle giving rise to the PSF of concern. This required establishing a conversion between radius and angle scales. This was readily obtained by convoluting mathematically the two normal distributions reported for R_{ves}[37] and R_{pore}.[22] The median opening angle value corresponding to the initial fusion pore opening (see Fig. 2B) could then be evaluated at $(\alpha_{pore}^{open})^{median} \approx 0.44^\circ$ (note that for the range of $(\alpha_{pore}^{open})^{median}$ values considered here, one has $\sin[\alpha_{pore}^{open}(\pi/180)]^{median} \approx (\pi/180)(\alpha_{pore}^{open})^{median}$ with ample accuracy). This value was taken as a normalization gauge used to derive a κ value from each experimental PSF current plateau through the following procedure.

The experimental current is proportional to the unknown C_{ves}^{rel} value. However, it may be readily shown (see Appendix) that:

$$Q/i_{pore} \approx (\pi/3)(R_{ves}^3/D_{ves}R_{pore}) = \pi/[3(\pi/180)\kappa\alpha_{pore}^{open}] = 60/(\kappa\alpha_{pore}^{open}) \quad (1)$$

so that equating α_{pore}^{open} to its gauge value (*viz.*, 0.44°) provided a first entry for κ which allowed disentangling of the problem from the unknown C_{ves}^{rel} value. This was further refined using a simulation program based on a specific conformal mapping allowing a fast and precise treatment of the high release flux near the edge of the fusion pore which enlarged with time[27] after specifically adapting it to very small angles. At each time step, an automatic feedback loop adjusted the time variations of $\alpha_{pore}(t)$ so that the simulated release flux tracked the experimental one, $\varphi(t) = i(t)/(2F)$ where $i(t)$ is the experimental amperometric current.[35] Such procedure generated a specific $\alpha_{pore}(t)$ function describing each single PSF event for the κ value used. Each $\alpha_{pore}(t)$ function displayed at least one plateau, α_{pore}^{open}. In cases where a series of successive plateaus was obtained (see below and Fig. 4) the one which immediately preceded the exponential growth phase (see the asterisk marks in Fig. 4) was considered as representative of the initial fusion pore. This procedure was automatically iterated through changing κ values up to when an α_{pore}^{open} resulted equal to the gauge one, $\alpha_{pore}^{gauge} = 0.44^\circ$. The above strategy was applied to a series of 80 representative amperometric events with PSFs of different shapes (*i.e.*, plateaux or ramps) and different magnitudes (*i.e.*, different $i_{pore}^{plateau}$ values) extracted from traces monitored on 5 batches of chromaffin cells with 7 μm diameter beveled carbon fiber ultramicroelectrodes according to a previously published procedure[30] (see the Experimental section and Fig. 2B).

Since we used a constant value for the gauge angle, this procedure led to a statistical distribution of 80 diffusion rate constant values (Fig. 3A). As expected for a series of single events, κ obeys closely an exponential distribution,[38a] *viz.*, $P(\kappa) = \exp(-\kappa/\kappa_{mean})/\kappa_{mean}$ with $\kappa_{mean} = 415\ s^{-1}$ representing the statistically significant mean κ value.[38b] Note that since $R_{ves}^{mean} = 156$ nm[37] it follows that the mean diffusion coefficient of neurotransmitter in the vesicle matrix, partially altered[39] near the pore entrance, is $D_{ves}^{mean} = 1.0 \times 10^{-7}\ cm^2\ s^{-1}$, *i.e.*, resulting in a value *ca.* 100 times smaller than in the extracellular medium. This justified *a posteriori* the assumption made in deriving eqn (A1)–(A3) in the Appendix, and hence validated our conclusion that the exact shape of the pore (*viz.*, toroid or tubular) was mostly irrelevant.

Each PSF was then re-analyzed imposing $\kappa_{mean} = 415\ s^{-1}$ as the common diffusion rate constant.[38b] This produced a distribution of α_{pore}^{open} values (Fig. 3B)

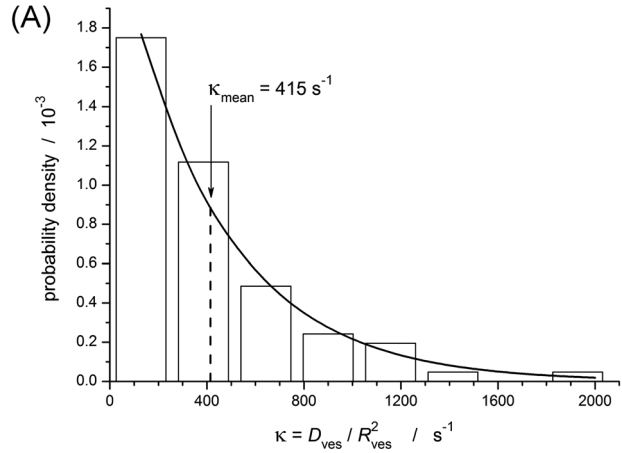

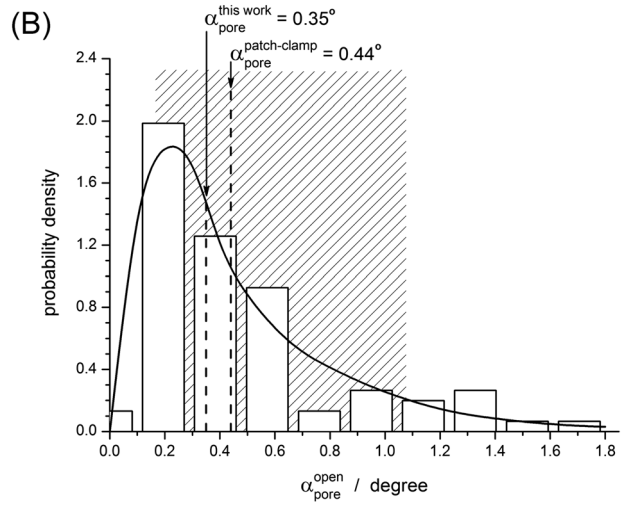

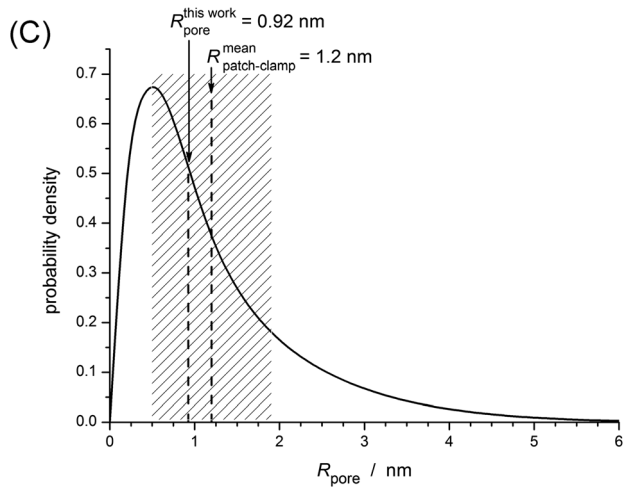

whose mean value was 0.35° instead of 0.44°, which was used for the gauge value. However, this apparent slight discrepancy was statistically insignificant; indeed, the present distribution was in perfect agreement with that predicted based on the analytical convolution between the distributions for patch-clamp (R_{pore}) and R_{ves} (Fig. 3B). Finally, convoluting the α_{pore}^{open} distribution with the reported R_{ves} normal one[37] afforded the distribution of R_{pore} values shown in Fig. 3C. This distribution also overlapped satisfactorily with that reported from patch-clamp measurements though it is more skewed towards high R_{pore} values.

The present analysis allowed the reconstruction of the opening time function of each initial fusion pore. Fig. 4 illustrates a few examples of such reconstructed time functions. Interestingly, some of these data show that the initial fusion pore may pass through two (*ca.* 10% of PSF) or even three (*ca.* 4% of PSF) stable successive stages during the pre-spike release, suggesting that the initial fusion pore does not always proceed irrevocably from its stable stage to its exponentially enlarging phase.[23,24,40–42] Such features were already present in the amperometric traces, though less noticeable due to their smearing out by the filtering effect of diffusion.[43] In this respect, the present analysis evidences that there is no fundamental difference between PSF with a plateau or ramp despite their experimental difference in shape.[30] To the best of our knowledge such a staircase transition of initial fusion pores towards their unstable state has never been reported before, except maybe in Fig. 2b of ref. 22, which reports one long patch-clamp trace with features which could be interpreted similarly. This may well represent progressive unlocking of SNARE assemblies[7] or changes of the membrane cytoskeleton[11,12] under the pressure created by the restrained swelling of the matrix near the pore entrance.[23,24,39] Alternatively, this may represent the progressive alteration of the matrix exposed to the extracellular medium (see below). However, the fact that there are no more than three such intermediate plateaus appears consistent with the SNAREs-related interpretation since three SNAREs complexes are supposed to be involved in the docking stage,[7] so that under some circumstances they may untangle sequentially within a few tens of milliseconds delay.

Most patch-clamp measurements indicate that initial fusion pores open suddenly.[4] Conversely, $\alpha_{pore}(t)$ time variations in Fig. 4 display rise times. Yet, this is not at all contradictory. Indeed, patch-clamp measurements involve electrokinetic measurements which track instantly (*i.e.*, are limited only by the experimental apparatus time constants which are exceedingly small)[15–17] any sudden changes in capacitance and resistance. Conversely, amperometry requires that molecules be released by the matrix and diffuse away.[44] Such a process cannot initiate before the matrix volume near the pore entrance has partially swollen,[23,24,39] so as to allow the neurotransmitter to achieve a sufficiently high diffusion coefficient compared to its restricted mobility in the initially highly compacted granule.

Fig. 3 Statistical distributions based on 80 amperometric events displaying well-defined PSF: (A) κ values as obtained through the normalization gauge procedure (see text); (B) α_{pore}^{open} as obtained through using a common diffusion rate constant value $\kappa_{mean} = 415\ s^{-1}$; (C) R_{pore} as obtained through the analytical convolution of α_{pore}^{open} distribution in (B) with that of R_{ves}[37] ($P(R_{pore}) = P(\alpha_{pore}^{open}) \otimes P(R_{ves})$). In (B,C) the hatched zones indicate the confidence intervals based on patch-clamp[22] and R_{ves}[37] published measurements (confidence levels: 95%). Values of $\alpha_{pore}^{this\ work}$ and $R_{pore}^{this\ work}$ are the medians of the respective distributions obtained in this work. Solid curves in (A) and (B) represent the statistical regressions determined based on the histograms. That in (C) results from the convolution between that in (B) with the normal distribution of vesicle radii.

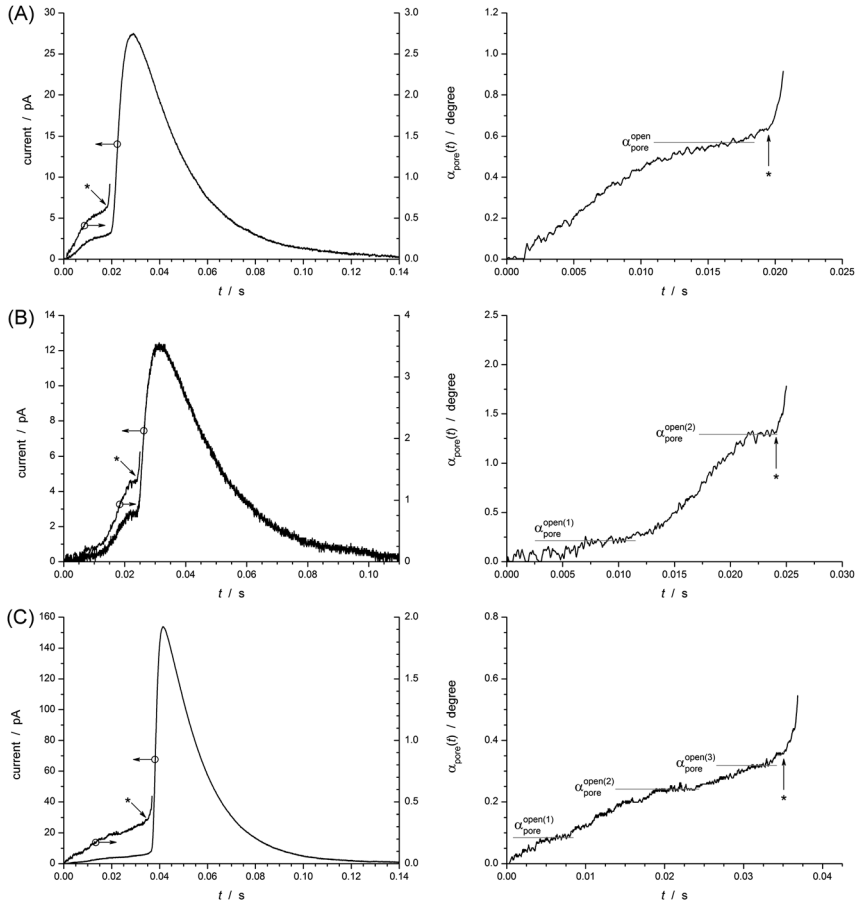

Fig. 4 Representative series of $\alpha_{pore}(t)$ time functions reconstructed using $\kappa = 415\ s^{-1}$ from a typical amperometric current trace exhibiting a well-defined PSF featuring single (A), double (B) and triple-stage (C) initial fusion pore transition towards the exponential growth phase (see insets). In each case the left column shows the actual current trace and the reconstructed $\alpha_{pore}(t)$ function while the right one gives an expanded view of it. For all reconstructed $\alpha_{pore}(t)$ time functions, the beginning of the exponential growth phase of the pores is indicated by an asterisk.

This process was shown to be fast[39a] but it cannot be instantaneous. Such a progressive local matrix distortion must thus appear as an apparent progressive increase in R_{pore} values in our analysis, which assumes a constant (*i.e.*, final) diffusion coefficient value at any time. As such, one may be tempted to conclude that the rise times shown in Fig. 4 feature an intrinsic bias in the present analysis and should then be discarded.[44] However, what matters biologically in the initial fusion pore opening is not really its opening but the flow of neurotransmitter it may release when it does so. Thus, rather than being an artifact, the rise times observed here provide extremely informative data on the biological role of fusion pores that patch-clamp measurements cannot. Although of extreme interest, a proper analysis of such phenomena is beyond the scope of this work and certainly requires an improvement in the time resolution of amperometric measurements (500 molecules per millisecond and a 25 μs sampling time at present).

Finally, and despite its excellent precision, it is noted that this analysis did not evidence initial fusion pore flickering or closing ("kiss-and-run" events).[3,22] The absence of "kiss-and-run" observation in our work follows obviously from the fact that, owing to the necessary use of eqn (1), all PSF which could be treated had to lead to full fusion, *i.e.*, had to be followed by a fully developed spike. However, one would think that flickering could be detected through our analysis. Yet, should a pore flicker, unless this led to a sufficiently long duration of the closed and open phases (*i.e.*, longer than a few milliseconds),[3] diffusional filtering in the matrix (see above) would necessarily average the open/closed phases into a lower and smoother PSF current.[44,45] If so, such events would then lead to smaller apparent values of $\alpha_{\mathrm{pore}}^{\mathrm{open}}$ and R_{pore} for such events, thus biasing the two distributions towards their low-value ranges.

Energy distribution of initial fusion pores

After the two membranes have partially fused so as to create a stable fusion pore, the dimensions of the latter are necessarily imposed by the energetics of the system whatever its initial energy and the constraints (biological or physicochemical) which apply on it and define its energy potential well. In this respect the initial pore system cannot differ from any other physicochemical one. However, there is one marked difference from usual physicochemical ones in the sense that the pore is created in a slow energy-dissipating environment. Usual quickly-deformable physicochemical systems may rapidly dissipate their excess energy by transfer into configuration changes and vibrations, solvent molecules vibrations, *etc.*, so that they may quickly equilibrate thermodynamically in their potential well. Conversely, irrespective of its toroid or tubular shape, the initial pore is created as a double-fold in a bilayer bilipidic membrane so that its capacity to release energy by usual means is drastically limited. Basically, it must dissipate its energy mostly through viscous transfer implying lateral shear friction of each monolayer against each other, since this is the only possibility for changing the double curvature of the pore. The same membrane displacements are also hampered viscously by the structured electrolyte surrounding it[23,24,40–42] and possibly by the membrane cytoskeleton mesh.[46] In addition, in the present biological case, such viscous dissipation may even be considerably reduced due to the presence of transmembrane proteins (including still locked SNAREs assemblies) which may restrict relative side-slipping of each membrane layer by clipping them locally, or owing to significant folding of the bilayer membrane.[18] As such, the initial fusion pore may maintain its initial energy for unusually long time durations compared to classical physicochemical systems (see the Appendix).

Despite these intrinsic differences, it remains that the statistical probability of observing a given initial pore, *i.e.*, with a given radius, depends on the energetic cost of creating such structure. Hence, the probability $P(R_{\mathrm{pore}})$ of observing a R_{pore} value in the distribution shown in Fig. 3C reflects the Boltzmann probability of achieving an overall energy $W_{\mathrm{pore}}(R_{\mathrm{pore}})$:[47]

$$P(R_{\mathrm{pore}}) \propto \exp[-\Delta W_{\mathrm{pore}}(R_{\mathrm{pore}})/k_{\mathrm{B}}T] \quad (2)$$

where k_{B} is the Boltzmann constant and T the temperature. This allows translation of the graph in Fig. 3C into the corresponding $\Delta W_{\mathrm{pore}}(R_{\mathrm{pore}})$ statistical variations shown in Fig. 5A which represents the variations of the initial fusion pore energy

with its radius. Note that in eqn (2) and hereafter we prefer using $\Delta W_{pore}(R_{pore})$ instead of $W_{pore}(R_{pore})$ to recall that this does not provide a proper energy scale but rather a relative one for the population at hand. In this context, let us stress upon one important caveat. Readers less familiar with physical electrochemistry may think that the electrode potential influences the pore energy, *e.g.*, contributing to partial electroporation, due to electrostatic interactions between cell membrane(s) and the electrode placed at sub-micrometric distances from the cell. However, in any electrolyte solution, such as PBS used here, and for electrode potentials up to several tenths of a volt, the electrostatic potential is screened over distances from the electrode surface less than one nanometer by appropriate ions. Hence, since the artificial synaptic cleft width is *ca.* 100 nm, the electrode potential cannot have any influence at all on the exocytotic process nor on the energy of the fusion pore. This electrochemical (Faradaic) situation differs considerably from those pertaining to electrophysiology which rely on so-called "reference electrodes" (*i.e.*, imposing a potential in its surroundings). Henceforth, what we consider in $W_{pore}(R_{pore})$ is the energy released into the system and not yet dissipated when the pore opens (see below and the Appendix).

Fig. 5A is constructed using an α_{pore}^{open} scale (*viz.*, based on the histogram distribution in Fig. 3B) rather than a R_{pore} one, since our analysis produced primarily α_{pore}^{open} values while the R_{pore} distribution in Fig. 3C was reconstructed statistically from the analytical fit of the α_{pore}^{open} one. Nonetheless, the plots in Fig. 5A & B provide approximate R_{pore} scales following a straight rescaling of the α_{pore}^{open} ones using: $<R_{pore}> \approx (156\pi/180)\alpha_{pore}^{open} \approx 2.72\alpha_{pore}^{open}$ where R_{pore} is in nm and α_{pore}^{open} in degrees).

Rapid inspection of the plot in Fig. 5A and comparison to those in Fig. 7 in the Appendix supports the view that the initial fusion pores have an essentially lipidic structure. To clarify this conclusion we need to briefly evoke the basic components which define the potential energy of bilayer membranes.[23,24,40–42] First, a pore of radius R_{pore} created in a partially tense lipidic membrane provides a decrease of the membrane surface area by πR_{pore}^2, and hence induces a decrease of its surface tension by $\Delta W_{tension} = -\sigma\pi R_{pore}^2$ (σ is the surface tension coefficient).[41] This tends to stabilize the system by enlarging the pore radius. However, by doing so imposes that a larger amount of lipids are transferred from the membrane bulk into unfavorable positions lying on the pore edge, thus increasing their energy proportionally to the pore perimeter, *i.e.*, by $\Delta W_{edge}^{line} = \rho(2\pi R_{pore})$ where ρ is the line tension coefficient.[41] Also, in a biological membrane, such expansion may confront some biological constraints (*e.g.*, still-locked SNAREs assemblies,[7] actin mesh of the cytoskeleton,[12,46] slow diffusing transmembrane proteins,[46] *etc.*). Altogether, this may create an additional positive "edge" energy, ΔW_{edge}^{biol}, also opposing the pore opening beyond a given radius (see the Appendix). Finally, when opened, the pore is prevented from closing spontaneously by several factors. First, decreasing the pore radius to extremely small values would necessarily imply a considerable equatorial bending of the membrane (*i.e.*, curvature centered on the symmetry axis of the pore) while this becomes negligible *vs.* the fold-bending at larger R_{pore} values whose effect on the energy was included in the ΔW_{edge}^{line} expression above. Second, facing membranes brought to angstromic distances from each other experience electrostatic or Van der Waals repulsions.[8] Third, closing up a nanometric pore requires squeezing out rather structured solvent molecules and electrolyte ions.[48] Except for the first one,[42] these

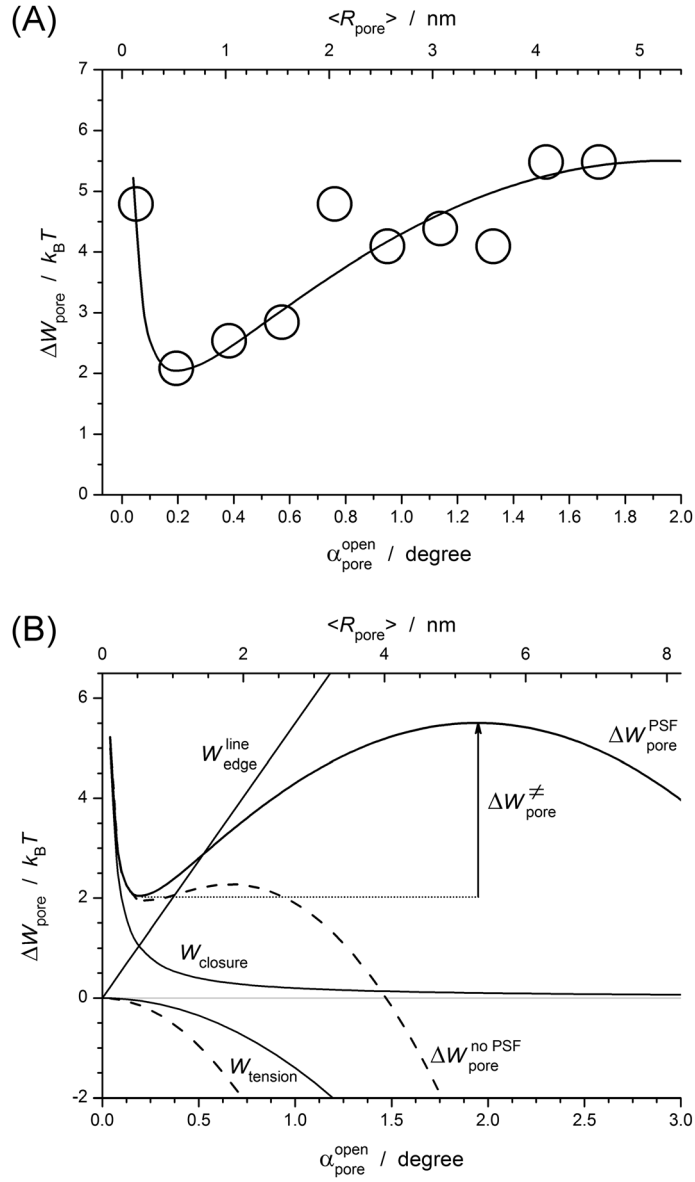

Fig. 5 (A) Experimental variation of the pore potential energy as a function of its opening angle assuming a Boltzmann control (eqn (2)) of the size distribution (open circles; each circle corresponds to one bin of the histogram in Fig. 3B and its fit according to eqn (3) (solid curve) with: $\gamma_{mean} = 2.2 \times 10^{-30}$ J m and $n = 1$, $\rho_{mean} = 1.3$ pN, $\sigma_{mean} = 0.25$ mN m^{-1}. (B) Individual components of the fitting equation in (A). In (A,B) the top horizontal axis shows a straight conversion of the α_{pore}^{open} bottom axis into the R_{pore} one using $<R_{pore}> = \alpha_{pore}^{open}(\pi/180)R_{ves}^{mean}$, where α_{pore}^{open} is in degrees, R_{pore} in nm and $R_{ves}^{mean} = 156$ nm.[37] In (B) the dashed curves correspond to the same γ_{mean} and ρ_{mean} values as the solid ones but to $\sigma_{mean} = 0.68$ mN m^{-1} (see text).

contributions are difficult to predict quantitatively in the absence of precise information on the pore structure. Yet, all three add collectively into an additional positive "edge" energy, $\Delta W_{edge}^{closure}$, prevailing at angstromic distances but vanishing after a few angstroms radius. In absence of any better knowledge one may

thus consider in a first approximation that $\Delta W_{edge}^{closure}$ varies as γ/R_{pore}^{n} where γ and n are two constants depending on the exact operating repulsive forces.

Altogether, these energy components define the potential well, $\Delta W_{pore}(R_{pore}) = (\Delta W_{edge}^{closure} + \Delta W_{edge}^{line} + \Delta W_{edge}^{biol} + \Delta W_{tension})_{R_{pore}}$, in which the pore lies depending on its initial energy. If rapid energy dissipation could occur, the pore would reach its stable radius value corresponding to the potential energy minimum such as $d\Delta W_{pore}/dR_{pore} = 0$ and $d^2\Delta W_{pore}/dR_{pore}^2 > 0$.[23,24,40,42] Fig. 7 in the Appendix represents the typical expected shapes of $\Delta W_{pore}(R_{pore})$ depending on the relative magnitudes of ρ/σ either in the absence (*viz.*, when ΔW_{edge}^{biol} is negligible *vs.* the other energies involved) or in the presence of biological edge constraints (*viz.*, when ΔW_{edge}^{biol} is significant). Comparison of the plot in Fig. 5A to those in Fig. 7 strongly suggests that the pore structure is mostly governed by its lipid-related energy components, *i.e.* that ΔW_{edge}^{biol} may be neglected. This is further supported by the decomposition of the regression energy curve into its three individual components as shown in Fig. 5B (arbitrarily using $n = 1$ in describing $\Delta W_{edge}^{closure}$, since there is not enough data in the pertinent range to estimate the n value):

$$\Delta W_{pore}^{lipid}(R_{pore}) = (\gamma/R_{pore}) + 2\pi\rho R_{pore} - \pi\sigma R_{pore}^2 \quad (3)$$

Analysis of the data in Fig. 5A according to eqn (3) yielded (correlation coefficient = 0.81, 80 PSF) $\gamma_{mean} = 2.2 \times 10^{-30}$ J m, $\rho_{mean} = 1.3$ pN and $\sigma_{mean} = 0.25$ mN m^{-1} for room temperature (*i.e.*, $k_BT = 4.1 \times 10^{-21}$ J). To the best of our knowledge it is impossible to evaluate the plausibility of the ensuing γ value whose precision is extremely low. However, rationalizing γ as mostly stemming from electrostatics[49] would imply considerably less than one elementary charge being located within the pore area. This result evidences that if any charges or dipoles do exist they are totally screened by the electrolyte.[49] Hence, such γ value seems more coherent with the assumption that $\Delta W_{edge}^{closure}$ features the squeezing of electrolyte ions and water molecules out of fusion pores.[48] Conversely, the above values for ρ and σ are determined with a rather good precision and are perfectly consistent with those reported for bilipidic membranes.[40,42]

To conclude this section we wish to discuss a specific aspect of the potential energy well shown in Fig. 5. Indeed, for the above σ and ρ values, a pore with an excess energy exceeding $\Delta W_{pore}^{\neq} \approx 3.5k_BT$ *vs.* the minimum of the potential well (at *ca.* $2k_BT$), *i.e.*, created with an initial radius larger than *ca.* 5.4 nm, should proceed immediately to its exponential growth phase since then $d\Delta W_{pore}/dR_{pore} < 0$ and increases in magnitude almost proportionally to R_{pore}. Conversely, pores created with a radius less than 5.4 nm should be poised in the potential well and be stable. In coherence with this analysis, the application of eqn (2) shows that 97% of the pores created under such conditions should be stable, a proportion which compares satisfactorily with the fact that, by construction, all the release events treated here gave rise to a PSF.

However, in normally tense bilipidic membranes σ may range up to 1 mN m^{-1} (and up to a few mN m^{-1} for tense ones; note however that above 10 mN m^{-1} bilipidic membranes cannot keep their cohesion and destructure by spontaneously creating pores to release their excess surface tension energy).[40,41] Thus, one may reasonably expect that among all release events (*i.e.*, including those which do not display a PSF) the initial pore may be created in membranes displaying a wider spectrum of surface tensions than those which led to the observation of PSF.

Experimentally it is commonly observed that *ca.* 70% of fusion events in chromaffin cells and related ones do not evidence any detectable PSF.[19,28] Within the framework of the present analysis, they correspond to an unstable initial fusion pore, *i.e.*, their 70% probability features that of the events giving rise to an activation barrier $\Delta W^{\neq}_{\mathrm{pore}}$ being less than $\Delta W^{\neq}_{\mathrm{pore}} < -(ln0.7)k_{\mathrm{B}}T \approx 0.36k_{\mathrm{B}}T$. Hence, assuming that the above ρ and γ values are constant features for the systems at hand, using eqn (3) leads to the prediction that whenever $\sigma \geq 0.68$ mN m^{-1} initial fusion pores are created under unstable conditions they proceed to their exponentially expanding phase from their very creation (compare Fig. 5B). Such a σ value is not unrealistic at all, being within the usual range of normally tense membranes, so this may well explain why *ca.* 70% of release events do not lead to any PSF observation.

Conclusion

The present work evidenced that, provided that external data entry is available, amperometric currents displaying a pre-spike feature (PSF) may be inverted theoretically so as to provide precise topological information about the initial fusion pores, *viz.*, about the crucial initial step which engages the full process of vesicular release. We choose here to rely on patch-clamp literature data on chromaffin cells as such an external input. This allowed evaluation of the diffusion rate, $\kappa = D_{\mathrm{ves}}/R^2_{\mathrm{ves}} = 415$ s^{-1}, of neurotransmitter cations in the partially altered matrix located near the pore entrance. In turn this led to an evaluation of the distribution of initial fusion pore radii and provided for the first time an experimental description of the potential energy well for such systems.

The shape of the corresponding potential energy well thus-reconstructed strongly suggests that after their creation initial fusion pores are essentially controlled by the usual physicochemical laws used in describing pores formed in bilayer lipidic membranes, *i.e.*, they have an essentially lipidic nature. This is an essential piece of information since there is still much debate about the structure of the initial fusion pores. Furthermore, upon assuming that the membranes may be partially tense, the conclusion of the energetic analysis performed here predicts that a rather large proportion of events should not lead to any thermodynamically stable fusion pores. This is fully coherent with the noted absence of any detectable PSF in 70% of amperometric events. Therefore, even if solving the inverse problem requires an external entry (taken here from patch-clamp literature data), the information contained in amperometric currents offer extremely important additional information.

Finally, assuming that the value of $\kappa = D_{\mathrm{ves}}/R^2_{\mathrm{ves}}$ remains constant[38b] for matrixes of chromaffin cells when "full" fusion occurs (*i.e.*, after the exponential growth phase of the fusion pore occurs), the same analysis may be extended so as to characterize the final extent of fusion pores at the end of their exponential growth phase. This would provide a first correct statistical evaluation of the extent of full fusion and afford a definitive answer to the question of how full "full" fusion is. Work is presently in progress in our laboratory in this direction.

Experimental

The 80 amperometric spikes with PSF analyzed here were extracted from amperometric traces of exocytosis monitored at Ba^{2+}-stimulated single bovine

chromaffin cells using beveled and polished carbon fiber ultramicroelectrodes (7-μm diameter). Details of electrode preparation and single cell experiments were identical to previously published procedures.[28] Electrodes were held at +0.65 V *versus* a silver/silver chloride reference electrode using a commercially available picoamperometer (model AMU-130, Radiometer Analytical Instruments, Copenhagen, Denmark) with a time response set at 50 μs. The output was digitized at 40 kHz, displayed in real time and stored on a computer (Powerlab-4SP A/D converter and software Chart, ADinstruments, Colorado Springs, CO) with no subsequent digital filtering. Each amperometric trace obtained during cell secretion was visually inspected and signals were marked as exocytotic spikes whenever their maximum current intensities were three times higher than the rms noise (0.4–0.7 pA), determined from the baseline current recorded before each signal (30 ms minimum time trace). Special attention was paid to verify the baseline stability before and after each spike to avoid any bias due to baseline drift. Overlapping spikes were excluded. Generally, 50–200 spikes fulfilling these criteria could be isolated from each amperometric trace, and among them only those displaying a clear PSF were retained. Signals from five different cell batches obtained from five different animals were gathered to produce the set of 80 spikes with PSF analyzed in this work.

Appendix

I. Influence of the shape of the pore: toroid *vs.* tubular

One expects intuitively that the exact shape of the pore, *viz.*, toroid or tubular (see Fig. 6) matters for the extraction of the opening angle from PSF currents, *i.e.*, conditions the validity of the present results. In fact, we show below that this is not true as soon as D_{ves}, the diffusion coefficient of the neurotransmitter in the altered part of the matrix near the pore entrance, is much smaller than its value, D_{cleft}, in the cleft of the artificial synapse (see Fig. 2B in the main text). Indeed, provided that the possible tubule length remains moderate, *viz.*, does not exceed a few tens of nanometers, for dense core vesicles such as those of chromaffin cells the only possible bias is that the D_{ves} value afforded by our toroid-based analysis may be slightly underestimated if a tubular connection was involved.

To establish this point let us evaluate the different diffusional fluxes of the neurotransmitter in all compartments that are visited when the pore is tubular (Fig. 6B). In the vesicle, owing to the relative values of the pore and vesicle radii (*i.e.*, *ca.* 1 nm *vs.* 150 nm), from the matrix side, the pore entrance can be viewed as creating a diffusional field akin to that of a disk nanoelectrode in an infinite insulating plane.[50] Indeed, the vesicle membrane curvature may be neglected with respect to the scales considered here. Furthermore, owing to the extremely short dimension scales considered here, steady state diffusion is achieved within microseconds. Thus:[50]

$$\phi_{ves} \cong 4D_{ves}(C_{ves}^{rel} - C_{ves}^{exit})R_{pore} \quad (A1)$$

where C_{ves}^{exit} is the neurotransmitter concentration in the matrix at the entrance of the pore and other variables are defined in the main text.

Considering a tubular pore of length L, the flux within the pore is given by:[31]

$$\phi_{pore} = \pi D_{pore}(C_{pore}^{enter} - C_{pore}^{exit})R_{pore}^2/L \quad (A2)$$

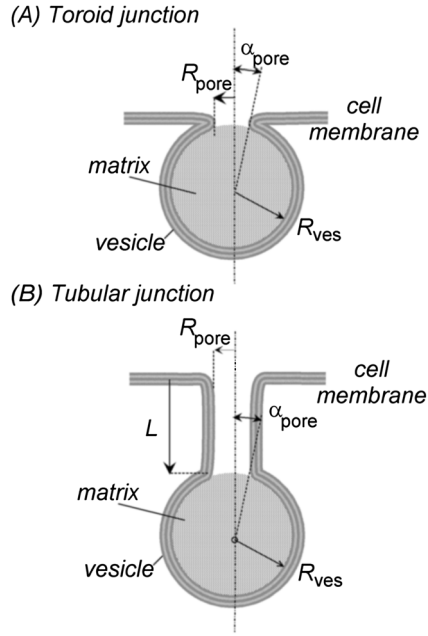

Fig. 6 Limiting geometries of the cell/vesicle membranes junction considered in this work: toroid (A) or tubular (B). Note that for the sake of simplicity and definition of the different variables used in the present model the pores are shown as being purely lipidic. Similarly, for clarity, the thickness of the membranes (*ca.* 3 nm) and the pore radius are enlarged with respect to the vesicle diameter.

where $C_{\text{pore}}^{\text{enter}} = C_{\text{ves}}^{\text{exit}}/\chi_{\text{matrix}}$ is the neurotransmitter concentration in the electrolyte at the pore entrance and $C_{\text{pore}}^{\text{exit}}$ that at its exit; χ_{matrix} is the partition coefficient of the neurotransmitter cation in the partially altered matrix (*i.e.*, smaller than that in the fully compact matrix which prevails before the pore is opened, but larger than in the fully swollen matrix).[34,39] D_{pore} is the diffusion coefficient of the neurotransmitter in the tubular pore. This may be considered as extremely close to its value, D_{cleft}, in the artificial synaptic cleft as soon as the pore diameter approaches or exceeds 2 nm.[51] Note that the expression for ϕ_{pore} in eqn (A2) considers only straight diffusion. Should an electroosmotic drive be also involved, owing to the direction of the pH gradient (*i.e.*, *ca.* 5.2 in the vesicle *vs.* physiological pH in the cleft),[52] a larger ϕ_{pore} would result. Hence, $(C_{\text{pore}}^{\text{enter}} - C_{\text{pore}}^{\text{exit}})$ would be smaller than predicted here considering the diffusional expression in eqn (A2) with the result that the pore length L would appear smaller. The ensuing analysis thus provides a maximum maximorum evaluation of the possible bias produced upon using a toroid junction based analysis instead of considering a tubular one when this applies. In other words, what follows evaluates the maximum distortion possibly incurred upon considering a toroid pore, when it may actually be tubular.

Since (i) the electrode maintains a zero concentration of neurotransmitter at its surface and (ii) the thickness of the cleft (*ca.* 100 nm) greatly exceeds the pore radius (a few nm at most), the flux inside the artificial synaptic cleft is again akin to that produced at a disk nanoelectrode.[50] Hence:

$$\phi_{\text{cleft}} = 4D_{\text{cleft}}C_{\text{pore}}^{\text{exit}}R_{\text{pore}} \quad \text{(A3)}$$

The three fluxes in eqn (A1)–(A3) are equal under steady state conditions so that: $\phi_{ves} = \phi_{pore} = \phi_{cleft} = i/(2F)$ where i is the monitored amperometric current.[35] This allows solving the system in eqn (A1)–(A3), from which it follows that:

$$i_{tube} = 8FD_{ves}C_{ves}^{rel}R_{pore}/\left[1 + \chi_{matrix}\frac{D_{ves}}{D_{cleft}}\left(1 + \frac{4L}{\pi R_{pore}}\right)\right] \quad (A4)$$

For a toroid pore, eqn (A2) does not apply since $L \approx 0$ and $C_{pore}^{enter} = C_{pore}^{exit} = C_{ves}^{exit}/\chi_{matrix}$, so that one obtains:

$$i_{tore} = 8FD_{ves}C_{ves}^{rel}R_{pore}/\left(1 + \chi_{matrix}\frac{D_{ves}}{D_{cleft}}\right) \quad (A5)$$

Comparing eqn (A4) and A5 shows that the two fluxes are strictly proportional and differ only by a correcting factor, *viz.*:

$$i_{tore} = i_{tube}(1 + \Gamma_{corr}) \quad (A6)$$

where:

$$\Gamma_{corr} = \left(\frac{4L}{\pi R_{pore}}\right)\Big/\left(1 + \frac{D_{cleft}}{\chi_{matrix}D_{ves}}\right) \quad (A7)$$

so that upon using a tore-based analysis instead of a tube-based one, when this applies, the only bias incurred is that D_{ves} value would need to be corrected to $D_{ves}^{tore}(1 + \Gamma_{corr})$ where D_{ves}^{tore} is that obtained through application of the tore-based model.

Though an upper boundary may be estimated for Γ_{corr}. Firstly, based on the results from Ewing *et al.*, which compared the mean neurotransmitter amounts released from fully swollen matrixes to those after normal exocytosis,[34] one may consider that a partially swollen matrix (*viz.*, still mostly constricted by its membrane) as considered here retains about 2/3 of its initial content (*i.e.*, leading to an amperometric current intensity lower than the baseline noise after 1/3 of its content has been released). This suggests that χ_{matrix} is at most a few units. Considering a toroid pore, our analysis showed that D_{cleft}/D_{ves} was close to 100. Hence, the expression of Γ_{corr} simplifies to:

$$\Gamma_{corr} = \frac{4}{\pi}\chi_{matrix}\frac{D_{ves}}{D_{cleft}} \times \frac{L}{R_{pore}} \quad (A8)$$

On the other hand, TIRFM experiments[4] evidence that fusing bulk vesicles are fully illuminated. Since vesicles have a diameter (*ca.* 300 nm) comparable to the length of the evanescent wave field, this shows that L/R_{ves} is much smaller than unity. Hence, L/R_{pore} is presumably at most a few tens. Therefore, even if the fusion pore has a tubular shape rather than a toroid one, Γ_{corr} is at most commensurable to a few units.

This ensures that considering a toroid connection instead of a possible tubular one does not affect at all the principle of our analysis. Furthermore, since we resorted to an independent entry (*viz.*, from published patch-clamp data) for calibrating R_{pore}, any possible bias incurred if Γ_{corr} was not negligible would be shifted onto the κ value reported in the text, which would be underestimated with respect to reality, but whose effect would be null due to the compensating auto-coherence of our analysis. For this reason, in the absence of precise independent

information on C_{ves}^{rel}, χ_{matrix}, D_{ves}/D_{cleft} and L/R_{pore}, we choose to rely on a tore-based model both for simplicity and to avoid the need to consider an additional unknown parameter (*viz.*, L/R_{ves} in our normalized framework).

II. Derivation of eqn(1) of the main text

The charge Q released by single vesicle and captured at the electrode surface is obtained upon integrating the amperometric spike current including the PSF. Hence, $Q = 4(2F)\pi R_{ves}^3 C_{ves}^{rel}/3$ (note that the electrooxidation of adrenaline is a two-electron process).[35] On the other hand, within the nanodisk analogy used here as a first analytical approximation, the current corresponding to the opened fusion pore is given by:[50] $i_{pore} = 4(2F)D_{ves}C_{ves}^{rel}R_{pore}$. A ratio of these two expressions readily affords:

$$Q/i_{pore} = \pi R_{ves}^3/(3D_{ves}R_{pore}) = \pi/[3(D_{ves}/R_{ves}^2) \times (R_{pore}/R_{ves})] \quad \text{(A9)}$$

which provides eqn (1) upon noting that $\kappa = D_{ves}/R_{ves}^2$ and $\alpha_{pore}^{open} = (180/\pi)R_{pore}/R_{ves}$, where α_{pore}^{open} is in degrees, as everywhere in the text.

III. Variations of the fusion pore energy *vs.* its radius in a lipidic pore

For the sake of simplicity, in eqn (3) we explained the different contributions to the initial fusion pore energy by considering the case of a purely lipidic structure since, ultimately, this is the relevant situation based on the present experimental and theoretical data. Under such circumstances, noting that the main influence of $\Delta W_{edge}^{closure}$ is restricted to sub-nanometric radii, while for non-tense membranes $\Delta W_{tension}$ and ΔW_{edge}^{line} act mostly at larger distances; in first approximation, the potential energy well (eqn (3)) displays a minimum at $R_{pore}^{min} \approx (\gamma/2\pi\rho)^{1/2}$ with $\Delta W_{pore}^{min} \approx 2(2\pi\rho\gamma)^{1/2}$ (for $n = 1$), and a maximum at $R_{pore}^{max} \approx \rho/\sigma$ with $\Delta W_{pore}^{max} \approx \pi\rho^2/\sigma$. Depending on the relative magnitudes of ρ and σ, the pore energy may be rather shallow (Fig. 7-IA), relatively well defined (Fig. 7-IB) or may even disappear if $\sigma > (2\pi\rho^3)/\gamma)^{1/2}$, *i.e.*, when the surface tension is high enough (*i.e.*, whenever σ approaches and exceeds 1 mN m^{-1} for the ρ and γ values obtained in Fig. 5).

When the potential energy well displays a local minimum at R_{pore}^{min} and a local maximum at R_{pore}^{max}, the energy difference $\Delta W_{pore}^{\neq} = \Delta W_{pore}^{max} - \Delta W_{pore}^{min}$ represents the activation energy required to rupture the initial fusion pore. Therefore, whenever $\Delta W_{pore}^{\neq} \gg k_BT$, after dissipating its initial energy, a pore of initial radius smaller than R_{pore}^{max} should rest around its stable minimum without any need for biological constraints to enforce such stability. Conversely, a pore created with an initial radius larger than R_{pore}^{max} should proceed spontaneously to its exponential growth while dissipating its initial energy.

While the pore is opened, catecholamine cations which maintain the cohesion of the intravesicular polyelectrolyte peptidic matrix through charge compensation and several hydrogen-bonds[53] are replaced by small hydrated cations to preserve electroneutrality. This provokes a trend for the matrix to swell.[39] On the other hand, while the pore is nanometric, most of the matrix remains necessarily enclosed in its membrane and swelling is drastically refrained. This situation forces the vesicle to equilibrate its swelling pressure by an increase of the surface tension of its membrane; hence, the tension coefficient σ necessarily increases with time.[23,24] From eqn (3) it is understood that this provokes a progressive

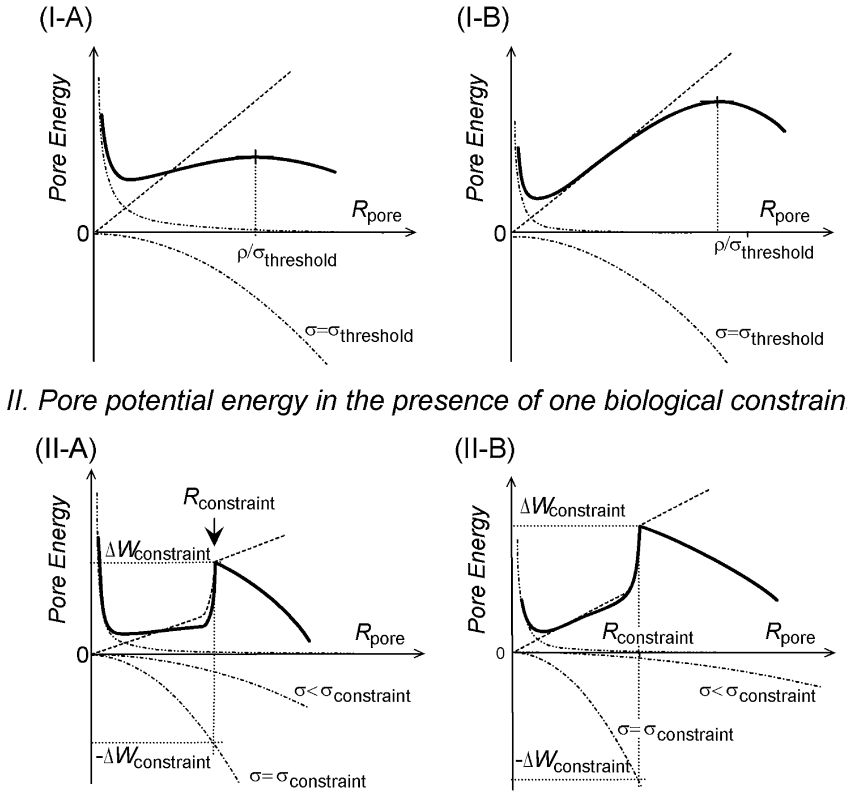

Fig. 7 Schematic potential energy of the initial fusion pore, for purely lipidic behavior (I), or when the pore is constrained by a biological structure or scaffolding (II); see text. In each case, situations featuring a low (A) or high (B) membrane tension relative to the pore edge one are represented. The overall energy is shown by the solid curve in each case together with its components: line edge energy (dashes), edge closure energy (dash–dot–dot), and surface tension energy (dash–dot); see text.

decrease of $\Delta W^{max}_{pore} \approx \pi\rho^2/\sigma$ and of $\Delta W^{\neq}_{pore} = \Delta W^{max}_{pore} - \Delta W^{min}_{pore}$. Therefore, provided it remains open for a sufficient time, any fusion pore will eventually reach a state in which $\Delta W^{\neq}_{pore} \cong k_BT$ or less so that it will irreversibly proceed to its exponentially expanding phase at a rate controlled by its energy dissipation[23,24,40,42] (see below, section V).

IV. Variations of the fusion pore energy *vs.* its radius in presence of biological constraints

Section III focused on a purely lipidic pore in which the line tension and surface tension energies scale as R_{pore} and R^2_{pore}, respectively.[23,24,40,42] However, in a biological membrane such as those considered here the situation may be far more complicated. Indeed, upon increasing its radius, the pore edge may meet some biological structure or scaffold which then should oppose its further expansion while the constraint holds. As a first approximation this can be represented as a sterical constraint applying for $R_{pore} \approx R_{constraint}$ and beyond.

The line tension energy may then be tentatively represented as being the sum of a linear contribution (*viz.*, $\approx 2\pi\rho R_{pore}$) and a Heaviside function (*viz.*, $\Delta W_{scaffold} \times \Theta[R - R_{pore}]$) so that $\Delta W_{edge}^{line} \approx 2\pi\rho R_{pore}$ when $R_{pore} < R_{constraint}$, while $\Delta W_{edge}^{line} \approx 2\pi\rho R_{pore} + \Delta W_{scaffold}$, when $R_{pore} \geq R_{constraint}$. Whenever $\Delta W_{constraint} = 2\pi\rho R_{constraint} + \Delta W_{scaffold}$ is not negligible *vs.* k_BT this situation leads to a characteristic energy profile which drastically differs from the potential energy well shape predicted for a purely lipidic pore (compare Fig. 7-IIA and 7-IIB).

Such biological constraints may involve still-locked SNAREs, actin meshes of the cell membrane cytoskeleton, transmembrane proteins locally nailing together the two bilayers, *etc.* Assuming that for $R_{pore} < R_{constraint}$ the pore still obeys a purely lipidic energy profile, the activation barrier limiting the pore widening beyond $R_{constraint}$ is $\Delta W_{pore}^{\neq} \approx \Delta W_{constraint} - 2(2\pi\rho\gamma)^{1/2}$. Hence, the pore expansion is stalled around $R_{constraint}$ up to when either the constraint disappears (*e.g.*, SNAREs unlocking, local reorganization of the membrane cytoskeleton,[11,12] *etc.*) or when the membrane surface tension energy increases sufficiently for the pore energy to overcome $\Delta W^{\neq}$ (see Fig. 7-II). Such a process may well repeat at a series of $R_{constraint}$ values when several constraints are met sequentially when the pore enlarges. This could explain the multi-step sequential opening of the initial fusion pore observed in this work (compare Fig. 4B,C).

V. Role of viscous dissipation on the kinetics of energy release

Initial fusion pores may be created only through overcoming the cell and vesicle membranes repulsion.[8,48] It is now widely accepted that the required energy is provided by the Ca^{2+}-mediated assembling of SNAREs complexes.[7] Seen in physicochemical terms, the situation is then akin to that of a chemical reaction which requires overcoming an activation barrier and then relaxation to a more stable state, *viz.*, here, that featuring the opened pore. Consequently, when this transition state is overcome the system necessarily possesses an excess energy with respect to the final pore potential energy well.[54,55] In any classical physicochemical non-structured environment, radiative energy transfer into molecular rearrangements and vibration modes of numerous chemical bonds rapidly dissipate this excess energy within a few picoseconds. However, this cannot occur so fast in a highly structured and viscous system with so few potentially vibrating bonds as the one at hand. Here, dissipation may occur mostly through structural deformations involving sliding of membrane bilipidic layers with respect to each other and with respect to the structured electrolyte bathing it.[23,24,40,42]

Hence, the pore dynamics (*viz.*, its ability to enlarge or close depending on its initial position *vs.* its local potential energy minimum and maximum, see below) is kinetically controlled by the rate at which its initial energy excess may be dissipated viscously. Denoting by η the two-dimensional viscosity of the system (note that the pore involves two curvature radii in orthogonal planes whatever its toroid or tubular shape), a purely lipidic pore thus experiences an algebraic growth of its radius given by:[23,24,40,42]

$$8\eta \frac{dR_{pore}}{dt} = -\frac{1}{2\pi}\frac{d\Delta W_{pore}}{dR_{pore}} = \sigma R_{pore} - \rho + \frac{\gamma}{2\pi R_{pore}^2} \quad \text{(A10)}$$

(using our above approximation, *viz.*, $W_{edge}^{closure} = \gamma/R_{pore}$). Thus:

$$\frac{dR_{pore}}{R_{pore}} = \frac{\sigma}{8\eta}\left\{1 - \frac{R_{pore}^{max}}{R_{pore}}\left[1 - \left(\frac{R_{pore}^{min}}{R_{pore}}\right)^2\right]\right\}dt \quad \text{(A11)}$$

where $R_{pore}^{min} \approx (\gamma/2\pi\rho)^{1/2}$ and $R_{pore}^{max} \approx \rho/\sigma$. Eqn (A11) shows that the pore should enlarge spontaneously towards R_{pore}^{min} when $R_{pore} < R_{pore}^{min}$ or towards large values when $R_{pore} > R_{pore}^{max}$, or decrease spontaneously towards R_{pore}^{min} when $R_{pore}^{min} < R_{pore} < R_{pore}^{max}$. However, these trends are regulated kinetically by the time constant $\tau = 8\eta/\sigma$, so they may be extremely slow in a non-highly-tense viscous membrane system as the one at hand ($\sigma \approx 0.25$ mN m^{-1}). For biological membranes $\eta \approx 10^{-6}$ N s m^{-1} appears a good average estimate for the two-dimensional viscosity,[42] so that τ is expected to fall in the range of several tens of milliseconds. Such a large time constant value with respect to the life-time of initial fusion pores is perfectly coherent with our observation that the initial fusion pores giving rise to PSF events did not relax during their life-time and remained distributed almost all over their potential energy well (compare Fig. 5A).

Acknowledgements

This work has been supported in part by the CNRS (UMR 8640), Ecole Normale Superieure (ENS, Paris), University Pierre and Marie Curie (UPMC), and the French Ministry of Research. The authors thank ANR (Chaire d'Excellence project "MicroNanoChem") and CNRS for financial support of this project in UMR 8640.

References and notes

1 R. D. Burgoyne and A. Morgan, *Physiol. Rev.*, 2003, **83**, 581–632.
2 A.-S. Cans, N. J. Wittenberg, R. Karlsson, L. Sombers, M. Karlsson, O. Orwar and A. G. Ewing, *Proc. Natl. Acad. Sci. U. S. A.*, 2003, **100**, 400–404.
3 See *e.g.*: (*a*) E. Neher, *Nature*, 1993, **363**, 497–498; (*b*) A. W. Henkel, H. Meiri, H. Horstmann, M. Lindau and W. Almers, *EMBO J.*, 2000, **19**, 84–93.
4 See *e.g.* among many TIRFM reports: (*a*) D. Zenisek, J. A. Steyer and W. Almers, *Nature*, 2000, **406**, 849–854; (*b*) J. G. Burchfield, J. A. Lopez, K. Mele, P. Vallotton and W. E. Hughes, *Traffic*, 2010, **11**, 429–439; (*c*) M. W. Allersma, L. Wang, D. Axelrod and R. W. Holz, *Mol. Biol. Cell*, 2004, **15**, 4658–4668.
5 L. J. Breckenridge and W. Almers, *Nature*, 1987, **328**, 814–817.
6 A. E. Spruce, L. J. Breckenridge, A. K. Lee and W. Almers, *Neuron*, 1990, **4**, 643–654.
7 R. Jahn and R. H. Scheller, *Nat. Rev. Mol. Cell Biol.*, 2006, **7**, 631–643.
8 D. Leckband and J. Israelachvili, *Q. Rev. Biophys.*, 2001, **34**, 105–267.
9 A. Gil, L. M. Gutierrez, C. Carrasco-Serrano, M. T. Alonso, S. Viniegra and M. Criado, *J. Biol. Chem.*, 2002, **277**, 9904–9910.
10 M. Criado, A. Gil, S. Viniegra and L. M. Gutierrez, *Proc. Natl. Acad. Sci. U. S. A.*, 1999, **96**, 7256–7261.
11 M. L. Gardel, J. H. Shin, F. C. MacKintosh, L. Mahadevan, P. Matsudaira and D. A. Weitz, *Science*, 2004, **304**, 1301–1305.
12 R. E. Guzman, P. Bolanos, A. Delgado, H. Rojas, R. DiPolo, C. Caputo and E. H. Jaffe, *Pfluegers Arch.*, 2006, **454**, 131–141.
13 J. Zimmerberg and K. Gawrisch, *Nat. Chem. Biol.*, 2006, **2**, 564–567.
14 J. B. Sorensen, *Annu. Rev. Cell Dev. Biol.*, 2009, **25**, 513–537.
15 E. Neher and B. Sakmann, *Nature*, 1976, **260**, 799–802.
16 O. P. Hamill, A. Marty, E. Neher, B. Sakmann and F. J. Sigworth, *Pfluegers Arch.*, 1981, **391**, 85–100.
17 E. Neher and A. Marty, *Proc. Natl. Acad. Sci. U. S. A.*, 1982, **79**, 6712–6716.
18 See *e.g.*: (*a*) E. Borroni, P. Ferretti, W. Fiedler and G. Q. Fox, *Cell Tissue Res.*, 1985, **241**, 367–372; (*b*) G. Q. Fox, *Cell Tissue Res.*, 1996, **284**, 303–316.
19 C. Amatore, S. Arbault, M. Guille and F. Lemaître, *Chem. Rev.*, 2008, **108**, 2585–2621.
20 M. Lindau and G. A. de Toledo, *Biochim. Biophys. Acta, Mol. Cell Res.*, 2003, **1641**, 167–173.
21 K. Lollike, N. Borregaard and M. Lindau, *J. Cell Biol.*, 1995, **129**, 99–104.

22 A. Albillos, G. Dernick, H. Horstmann, W. Almers, G. A. deToledo and M. Lindau, *Nature*, 1997, **389**, 509–512.
23 C. Amatore, Y. Bouret, E. R. Travis and R. M. Wightman, *Angew. Chem., Int. Ed.*, 2000, **39**, 1952–1955.
24 C. Amatore, Y. Bouret, E. R. Travis and R. M. Wightman, *Biochimie*, 2000, **82**, 481–496.
25 T. J. Schroeder, R. Borges, K. Pihel, C. Amatore and R. M. Wightman, *Biophys. J.*, 1996, **70**, 1061–1068.
26 F. Segura, M. A. Brioso, J. F. Gómez, J. D. Machado and R. Borges, *J. Neurosci. Methods*, 2000, **103**, 151–156.
27 (*a*) C. Amatore, A. I. Oleinick and I. Svir, *ChemPhysChem*, 2010, **11**, 149–158; (*b*) C. Amatore, A. I. Oleinick and I. Svir, *ChemPhysChem*, 2010, **11**, 159–174.
28 C. Amatore, S. Arbault, I. Bonifas, Y. Bouret, M. Erard, A. G. Ewing and L. A. Sombers, *Biophys. J.*, 2005, **88**, 4411–4420.
29 C. Amatore, S. Arbault, I. Bonifas, M. Guille, F. Lemaître and Y. Verchier, *Biophys. Chem.*, 2007, **129**, 181–189.
30 C. Amatore, S. Arbault, I. Bonifas and M. Guille, *Biophys. Chem.*, 2009, **143**, 124–131.
31 J. Crank, *The Mathematics of Diffusion*, 2nd edn, Oxford University Press, Oxford, 1975.
32 See *e.g.*: C. Amatore, Y. Bouret, E. Maisonhaute, J. I. Goldsmith and H. D. Abruña, *Chem.–Eur. J.*, 2001, **7**, 2206–2226.
33 B. Farell and S. J. Cox, *Bull. Math. Biol.*, 2002, **64**, 979–1010.
34 See *e.g.*: D. M. Omiatek, Y. Dong, M. L. Heien and A. G. Ewing, *ACS Chem. Neurosci.*, 2010, **1**, 234–245.
35 For the factor 2 (*i.e.*, two-electron overall route during electrooxidation of adrenaline under amperometric conditions), see: E. L. Ciolkowski, K. M. Maness, P. S. Cahill, R. M. Wightman, D. H. Evans, B. Fosset and C. Amatore, *Anal. Chem.*, 1994, **66**, 3611–3617.
36 A. Meunier, O. Jouannot, R. Fulcrand, I. Fanget, M. Bretou, E. Karatekin, S. Arbault, M. Guille, F. Darchen, F. Lemaître and C. Amatore, *Angew. Chem., Int. Ed.*, 2011, **50**, 5081–5084.
37 R. E. Coupland, *Nature*, 1968, **217**, 384–388.
38 (*a*) D. T. Gillespie, *J. Phys. Chem.*, 1977, **81**, 2340–2361; (*b*) It may be surprising that this analysis evidenced that $\kappa = D_{ves}/R_{ves}^2$ was a constant while R_{ves} exhibits a large distribution[37] (hence also D_{ves}). However, a plausible rationale for this fact is that the larger the vesicle, the larger the volume allowed to the matrix partial swelling. Since the volume expansion dV of the matrix resulting from a variation dR of its radius (allowed by the pore opening and increase in the membrane tension) is $dV/dR = 4\pi R^2$, it seems reasonable to consider that the change in diffusion coefficient scales with R_{ves}^2. Indeed in the partially swollen matrix, neurotransmitters certainly mostly diffuse through the altered zones; see, *e.g.*: C. Amatore, R. S. Kelly, E. W. Kristensen, W. G. Kuhr and R. M. Wightman, *J. Electroanal. Chem.*, 1986, **213**, 31–42.
39 (*a*) C. Nanavati and J. M. Fernandez, *Science*, 1993, **259**, 963–965; (*b*) J. Zimmerberg, M. Curran, F. S. Cohen and M. Brodwick, *Proc. Natl. Acad. Sci. U. S. A.*, 1987, **84**, 1585–1589; (*c*) P. E. Marszalek, B. Farrell, P. Verdugo and J. M. Fernandez, *Biophys. J.*, 1997, **73**, 1160–1168; (*d*) P. E. Marszalek, B. Farrell, P. Verdugo and J. M. Fernandez, *Biophys. J.*, 1997, **73**, 1169–1183.
40 O. Sandre, L. Moreaux and F. Brochard-Wyart, *Proc. Natl. Acad. Sci. U. S. A.*, 1999, **96**, 10591–10596.
41 C. Taupin, M. Dvolaitzky and C. Sauteret, *Biochemistry*, 1975, **14**, 4771–4775.
42 Y. A. Chizmadzhev, P. I. Kuzmin, D. A. Kumenko, J. Zimmerberg and F. S. Cohen, *Biophys. J.*, 2000, **78**, 2241–2256.
43 T. J. Schroeder, J. A. Jankowski, K. T. Kawagoe, R. M. Wightman, C. Lefrou and C. Amatore, *Anal. Chem.*, 1992, **64**, 3077–3083.
44 The rise-times cannot be due to the diffusion between the initial fusion pore and the electrode surface, since in the "artificial synapse" configuration[16] the latter is placed within a few hundred nanometers of the cell membrane. Hence, diffusion of released neurotransmitters over the artificial synaptic cleft was faster than a few microseconds and could not lead to the observation of the recorded rising times. Similarly, the sampling time resolution was 25 μs so this could be an instrumental artifact.
45 However, it must be noted that very few papers report observation of initial fusion pores flickering in amperometric traces; see *e.g.*: (*a*) Z. Zhou, S. Misler and R. H. Chow, *Biophys. J.*, 1996, **70**, 1543; (*b*) R. G. W. Staal, E. V. Mosharov and D. Sulzer, *Nat. Neurosci.*, 2004, **7**(4), 341. Yet, it is not yet a clear case and, beyond the authors' claims, the possibility remains that such observations resulted from accidental spike superimposition (Zhou *et al.*) or could be a very specific feature pertaining to cell models different from chromaffin cells, producing sufficiently long-lasting initial fusion pores with long periods of opening and closing so as to be not filtered by diffusion (Staal *et al.*).

46 (*a*) A. Kusumi, Y. Umemura, N. Morone, T. Fujiwara, in *Anomalous Transport: Foundations and Applications*, ed. R. Klages, R. Radons and I.M. Sokolov, Wiley, New York, 2008; (*b*) A. Kusumi, C. Nakada, K. Ritchie, K. Murase, K. Suzuki, H. Murakoshi, R. S. Kasai, J. Kondo and T. Fujiwara, *Annu. Rev. Biophys. Biomol. Struct.*, 2005, **34**, 351–378; (*c*) A. Kusumi and Y. Sako, *Curr. Opin. Cell Biol.*, 1996, **8**, 566–574; (*d*) H. Murakoshi, R. Iino, T. Kobayashi, T. Fujiwara, C. Ohshima, A. Yoshimura and A. Kusumi, *Proc. Natl. Acad. Sci. U. S. A.*, 2004, **101**, 7317–7322.
47 L. D. Landau and E. M. Lifshitz. *Statistical Physics*, vol. 5, 3rd edn, Pergamon Press, Oxford, 1980.
48 J. Klein and E. Kumacheva, *J. Chem. Phys.*, 1998, **108**, 6996–7009.
49 C. Amatore, A. Oleinick and I. Svir, *ChemPhysChem*, 2009, **10**, 211–221.
50 C. Amatore, A. I. Oleinick and I. Svir, *J. Electroanal. Chem.*, 2006, **597**, 69–76.
51 C. Amatore, *Chem.–Eur. J.*, 2008, **14**, 5449–5464, and references therein.
52 C. Amatore, S. Arbault, Y. Bouret, M. Guille and F. Lemaître, *ChemPhysChem*, 2010, **11**, 2931–2941.
53 J. L. Barrat and J. F. Joanny, Theory of polyelectrolyte solutions in *Advances in Chemical Physics*, ed. I. Prigogine and S. Rice, Vol. XCIV, Wiley, New York, 1966, pp. 27–33.
54 R. Long, C.-Y. Hui, A. Jagota and M. Bykhovskaia, *J. R. Soc. Interface*, 2012, **9**, 1555–1567.
55 The Gaussian curvature (see: U. Seifert and R. Lipowsky, in Structure and Dynamics of Membranes, From Cells to Vesicles, ed. R. Lipowsky and E. Sackmann, Elsevier, Amsterdam, 1995, pp. 409–411), contributes also to the initial energy of the fusion pore. The modulus of Gaussian curvature energies is predicted to be about $300k_BT$.